Nanoscale

PAPER

View Article Online
View Journal | View Issue

High sensitivity molecule detection by plasmonic nanoantennas with selective binding at electromagnetic hotspots

Cite this: *Nanoscale*, 2014, **6**, 1416

Nan Zhang,[a] Yan Jun Liu,[a] Jing Yang,[b] Xiaodi Su,[a] Jie Deng,[a] Chan Choy Chum,[a] Minghui Hong[b] and Jinghua Teng*[a]

Received 23rd August 2013
Accepted 24th October 2013

DOI: 10.1039/c3nr04494g

www.rsc.org/nanoscale

We report a highly sensitive biomolecule detection by plasmonic nanoantenna arrays with selective binding at the optical hotspots. The plasmonic nanoantennas consist of two separated Au nanorods with a thin Ti disk placed in between. By using selective surface modification chemistry, controlled binding occurs only in the gaps between the plasmonic nanoantennas, which ensures a high detection sensitivity. Both optical characterization using a dark field microscope and the FDTD simulation show that after the streptavidin binding, the signal increases with decreasing gap size. Compared to a single nanorod, the signal obtained per bound molecule in the nanoantennas increases by a factor of six, which is promising with respect to the future detection of single molecules.

1. Introduction

The surface plasmon resonance phenomenon in metallic nanostructures has been extensively studied and applied to enhance fluorescence[1–4] and Raman scattering,[5–8] color filtering,[9–12] nano-optical lithography,[13–15] solar energy harvesting,[16] and biological and chemical sensing.[17–19] This strong field confinement originating from the localized surface plasmon resonance (LSPR) creates electromagnetic hotspots around the metallic nanostructures. When light interacts with the metallic nanostructures, the conduction electrons oscillate collectively at a resonant frequency that depends on the size, shape, and composition of the metallic nanostructure. The inter-coupling between the metallic nanostructures and the polarization of the incident light also affect the LSPR peak. In the LSPR mode, the nanostructures absorb and scatter light intensely so that a single nanostructure or nanoparticle can be observed by dark-field microscopy.[20,21] Among various plasmonic nanostructures, the dipole nanoantenna, *i.e.* a pair of metal nanoparticles spaced by a nanometric gap, has been attracting significant attention due to its huge field enhancement in the gap, creating a hotspot due to the strong coupling between the dipolar LSPRs of each particle when they are brought close to one another in a dimer configuration. It has been shown that the electric field localized at the hotspots can lead to a field enhancement of two orders of magnitude at the resonance frequency.[22] Moreover, the resonance frequency of plasmonic dipole antennae can be tuned to a desired value by varying the antenna length or gap size, providing additional design flexibility.[23] Optoelectronic devices have taken advantage of the dipole nanoantennas configuration, for example as emitters and detectors.[24,25]

It is known that the plasmon resonance of a metallic nanoparticle is highly sensitive to the refractive index change of the surrounding medium, which is the underpinning principle of plasmonic label-free biosensing. When biomolecules with a higher refractive index than the surrounding medium bind to metal nanoparticles, the increase in the local refractive index will cause a spectral red-shift in the extinction or scattering spectra. This is analogous to classical label-free surface plasmon resonance (SPR) biosensors based on the surface plasmon polariton (SPP) excited at the metal/dielectric interface. The propagating SPP can probe hundreds of nanometers into the medium,[26] whereas the LSPR typically only probes tens of nanometers into the medium.[27] The longer field extension in the SPR accounts for the 10–100 times higher sensitivity of the medium's bulk refractive index change compared to the LSPR.[28] However, as most biomolecular analytes have a size of only a few nanometers, only a small fraction of the intense fields is utilized in SPR. In contrast, LSPR sensors possess probing volumes that better match the size of biomolecules, and the electric field enhancement around the metal nanoparticles is much larger than that of SPR sensors. Thus, they are expected to have a much higher surface sensitivity. A great potential associated with the localized nature of LSPR is the possibility to create miniature sensors with multiplex measurements. For this purpose, molecular binding to single nanoparticles has been investigated by several groups,[29–34] demonstrating detectable signals from a few hundred protein molecules.

[a]*Institute of Materials Research and Engineering, Agency for Science, Technology and Research (A*STAR), 3 Research Link, Singapore 117602. E-mail: jh-teng@imre.a-star.edu.sg; Fax: +65 6872 7528; Tel: +65 6874 8590*

[b]*Department of Electrical and Computer Engineering, National University of Singapore, Singapore 117576*

Since the LSPR based sensing mechanism is highly associated with the electric field distributions, the sensitivity is usually distributed inhomogeneously on the sensor elements. This is particularly apparent for optically coupled plasmonic nanoantennas. In such a system, the hotspot locates in between the nanoparticles (*i.e.* in the gap region), showing extremely high sensitivity, while other regions provide significantly lower/neglectable sensitivity accordingly. An improvement in the limit of detection can be obtained by directed molecule binding to the high-sensitivity areas.[35,36]

In this work, we demonstrate hybrid plasmonic nanoantenna arrays for biosensing application, with a selective biomolecule binding strategy to enhance the sensitivity. The hybrid plasmonic nanoantennas with a 10 nm thick Ti disk situated in the gap between a pair of Au nanorods were fabricated by electron beam lithography (EBL) and the biosensing experiments were studied by using dark-field microspectroscopy. Material selective surface modification chemistry was used to direct the biomolecular binding solely onto the Ti disk in the gap of the nanoantenna, leaving other regions unbound. Experimental results show that our hybrid plasmonic nanoantenna arrays have greatly enhanced sensitivity, moving one step further towards single-molecule detection.

2. Materials and methods

Materials

Thiol-poly(ethylene glycol)-biotin (SH-PEG–biotin, MW: 5 kDa) and thiol-poly(ethylene glycol) (SH-PEG, MW: 5 kDa) were purchased from NANOCS (United States), poly(L-lysine)-*graft*-poly(ethylene glycol) (PLL–*g*–PEG, PLL MW: 20 kDa, PEG MW 2 kDa, the number of lysine units per grafted PEG chain was 3.5) and nitrodopamine–poly(ethylene glycol)–biotin (ND–PEG–biotin) were purchased from SuSoS (Switzerland). Phosphate Buffered Saline (PBS) buffer, 3-(*N*-morpholino)propanesulfonic acid (MOPS), K_2SO_4, NaCl, Na_2SO_4 and streptavidin were purchased from Sigma-Aldrich (Singapore).

Sample fabrication

Nanoantenna arrays were fabricated on a quartz substrate by EBL. A 170 nm thick ZEP-520A resist was spin-coated onto a glass substrate. The ZEP-520A resist was baked at 180 °C for 2 min. Designed patterns were exposed at a dose of 320 μC cm^{-2} by using an electron beam with acceleration voltage of 100 kV and a beam current of 50 pA. The exposed samples were developed in *O*-xylene for 30 s and then rinsed in IPA for 20 s. After metal deposition, the lift-off process was carried out by soaking the sample in Remover 1165 overnight. The sample was then rinsed with IPA and deionized water, and blown dry with nitrogen gas.

Gold was selected as the material of our nanoantennas due to its excellent chemical stability and the matured Au–thiol binding chemistry in surface modification. To position the Ti disks at the hotspots of the Au nanoantennas, the alignment markers were first defined on the quartz substrate using EBL. Then, the Ti disks and the Au nanoantennas were fabricated in two separate cycles. In the first cycle, a square pattern of 60 nm × 60 nm was written according to the alignment marker position. A 10 nm Ti film was deposited by electron beam evaporation, followed by a lift-off process. Similarly, in the second cycle, a nanoantenna was fabricated with an Au thickness of 50 nm (with a 2 nm Cr adhesion layer). As control samples, Au nanorods and nanoantennas without Ti disks were fabricated at the same time in the second cycle.

The surface morphologies of the fabricated samples were characterized using a field emission scanning electron microscope (FESEM). A very thin Pt film was coated onto the samples to prevent the charging effect during SEM testing.

Surface modification and streptavidin binding

All samples had their surfaces treated with O_2 plasma after the fabrication process to ensure the complete removal of resist residuals. The surfaces of the Ti disks of the hybrid nanoantenna samples spontaneously transformed into TiO_2 after exposure to air.[37] The nanoantenna samples were modified in three steps. First, the samples were exposed to the SH-PEG (the PEG-terminated alkanethiol) solution (0.5 mg ml^{-1} in 0.01 M PBS buffer) for 1 h, followed by rinsing with PBS buffer and deionized (DI) water, and blow drying with nitrogen gas. The SH-PEG binds to gold surfaces, but does not adsorb on SiO_2 or TiO_2 surfaces. Second, the sample was incubated in the ND–PEG–biotin solution at 60 °C for 4 h (0.1 mg ml^{-1} in 0.1 M MOPS buffer, pH = 6, with 0.6 M K_2SO_4 and 0.6 M NaCl), followed by rinsing in DI water and overnight immersion in PBS buffer to remove weakly bound molecules. ND–PEG–biotin was adsorbed onto TiO_2 exclusively in this step. Third, the remaining SiO_2 surface was backfilled with PLL–*g*–PEG (0.1 mg ml^{-1} in PBS buffer) for 30 min, to avoid unspecific binding of proteins to SiO_2 regions, followed by rinsing with PBS buffer and DI water, and then blow drying with nitrogen gas.

The sample surface of the nanorods was modified in two steps: first, the surface was exposed to an SH-PEG–biotin solution (0.5 mg ml^{-1} in 0.01 M PBS buffer) for 1 h, followed by rinsing with PBS buffer. Second, the surface was exposed to the PLL–*g*–PEG solution (0.1 mg ml^{-1} in PBS buffer) for 30 min, followed by rinsing with PBS buffer and DI water, and then blow drying with nitrogen gas.

Streptavidin was dissolved in PBS at a concentration of 500 nM. The samples were incubated with the streptavidin solution under steady conditions for 30 min, followed by rinsing with PBS and DI water, and then blow drying with nitrogen gas.

Dark-field microscope measurement

An Olympus IX 71 inverted optical microscope equipped with standard dark-field (DF) condenser and spectrometer was used for the optical measurements, including the optical image and spectrum recording of elastic scattering from the samples. A dry DF condenser (NA = 0.8–0.92) was used to focus the un-polarized white light onto the sample and a 20× objective lens (NA = 0.5) was employed to collect the scattering spectra and DF images through a spectrometer and CCD camera, respectively.

Numerical simulation

Lumerical FDTD solutions were used for the 3D finite-difference time-domain (FDTD) simulations. The scattering cross section spectra of the designed structures were studied. A total field scattered field (TFSF) plane wave was applied as the source. Perfect matched layers were used as an effective absorbing boundary condition to investigate the individual behavior of the nanoantennas.

The dielectric functions of Ti, Cr and quartz substrate were obtained from Palik's book.[38] The dielectric functions of Au structures were obtained from the experimental data of Johnson and Christy.[39] The refractive index of the molecular layer and the streptavidin are 1.48 (ref. 40) and 1.45 (ref. 41), respectively.

3. Results and discussion

Three different nanostructures were applied in this work, whose schematic structures are illustrated in Fig. 1(a). The left column shows the hybrid nanoantenna, which consists of two separated Au nanorods with a thin Ti disk placed in between. After the surface modification, the Au and SiO_2 surfaces were deactivated by SH-PEG and PLL–*g*–PEG,[42] respectively. The biotin functional group was introduced onto the TiO_2 surface through the use of ND–PEG–biotin. The attachment strategy of the ND–PEG–biotin binding to the TiO_2 surface is based on catecholic chemistry, where nitrodopamine (ND) binds to the TiO_2 surface *via* the catechol group. In terms of the binding of metal cations to the TiO_2 surface, two coordination schemes can come into play: monodentate bonding or mixed monodentate-bidentate bonding.[43] Due to the different isoelectric points (IEP) of SiO_2 and TiO_2, the biotin functional group is introduced onto the TiO_2 surface exclusively.[44] After the streptavidin incubation, the protein will bind to the gap of the nanoantenna due to the high affinity specific biotin–streptavidin binding.[45] As the negative control experiment for the streptavidin binding, the nanoantennas without a Ti disk underwent the same surface modification as that of the hybrid nanoantennas, which is shown in the middle column in Fig. 1(a). Another control experiment was carried out on a single nanorod whose surface was modified by SH-PEG–biotin, shown in the right column in Fig. 1(a). After streptavidin incubation, the protein will bind to the whole surface of the Au nanorod.

The hybrid nanoantenna was characterized before the surface modification. Fig. 1(b) shows a dark-field image and the representative SEM image of a plasmonic nanoantenna array. The nanoantennas with controllable gap size were formed by two Au nanorods with a size of 55 nm × 110 nm and a metal thickness of 50 nm. The distance between neighboring nanoantenna structures is 5 μm. Each nanoantenna appears as a diffraction-limited light source. A reddish color corresponding to light scattered by individual nanoantenna was observed under DF illumination. Fig. 2(a) and (b) show the measured and simulated scattering spectra for two hybrid nanoantenna arrays with gap sizes of 20 nm and 45 nm, respectively. We can see that with decreasing gap size, there is a red shift of the resonance peak wavelength both in measured and simulated scattering

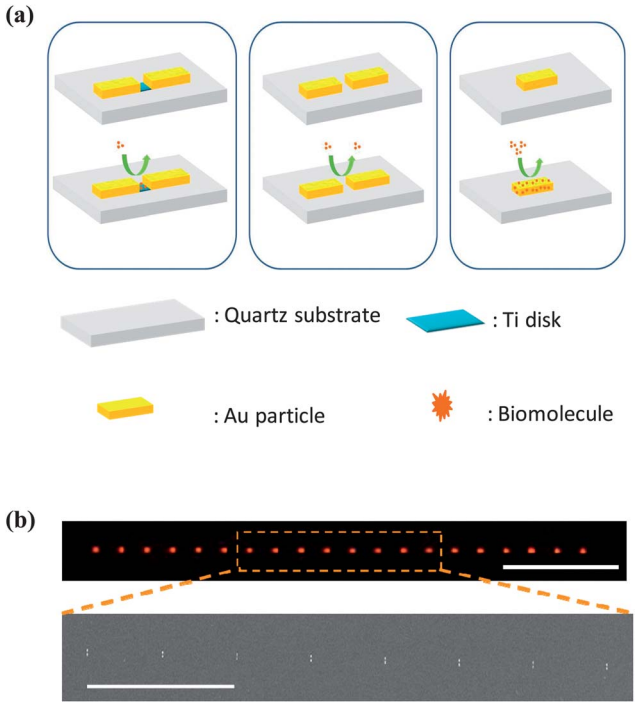

Fig. 1 (a) Schematic illustration of the biomolecular binding on the different nanostructures and (b) representative dark-field and corresponding SEM images of hybrid nanoantennas. Scale bars in the dark-field and SEM images are 20 μm and 10 μm respectively.

spectra. The scattering spectra in Fig. 2(a) were measured using unpolarized light. Under un-polarized light, the dipole nanoantennas present two resonances with one at low energy for excitation along the long axis of the dimer (longitudinal mode) and one at higher energy for excitation perpendicular to the long axis of the dimer (transverse mode). In the case of our nanoantenna structures, the scattering cross-section under transverse polarization is much smaller than that of longitudinal polarization. Thus, the superposition of the two resonances makes the shape of the resonance obtained a little bit asymmetric, as seen in the measured scattering spectra in Fig. 2(a). In the simulated scattering spectra in Fig. 2(b), longitudinally polarized light was applied to clearly show the surface plasmon resonance effect in the scattering spectrum. Fig. 2(c) is the simulated electric field intensity distribution at the resonance wavelength. The mappings were created by sampling the near-field region of the nanoantenna excited by longitudinally polarized light. In the gap region, the LSPRs couple with each other and lead to greatly enhanced field intensities at the hotspots. From Fig. 2(c), we can also clearly see that the electric field intensity at the hotspots increases with decreasing gap size as the plasmon coupling becomes stronger for a smaller gap size.

We chose biotin–streptavidin affinity binding for the biosensing investigation. Fig. 3(a) shows the scattering spectra of the biotin functionalized hybrid nanoantenna array with a gap size of 20 nm, before and after the streptavidin binding. After the streptavidin binding, a clear LSPR peak red shift of 8 nm is observed in the spectra. A control experiment using a

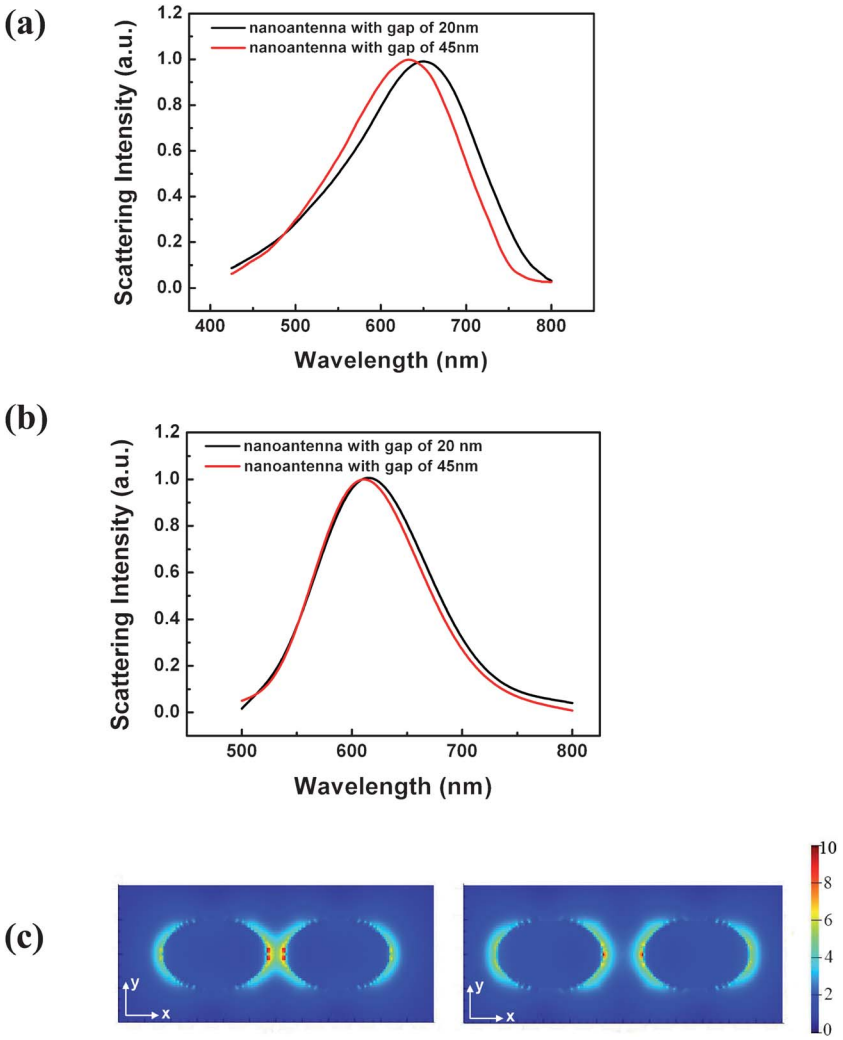

Fig. 2 (a) Experimental and (b) simulated optical scattering, and (c) electric field distributions of the nanoantenna arrays with different gap sizes (20 and 45 nm) before surface modification at longitudinal polarization light illumination (E-field along *x* direction), for the gap of 20 nm at a resonance wavelength of 642 nm (left), and for the gap of 45 nm at resonance wavelength of 635 nm (right).

nanoantenna array without a Ti disk was also carried out, as shown in Fig. 3(b). There is no clear peak shift observed, indicating that the red shift in the hybrid nanoantenna array results from selective streptavidin binding. This low unspecific binding response also proves that both SH-PEG and PLL–*g*–PEG are efficient in the prevention of unspecific protein adsorption. Fig. 3(c) shows the simulated optical responses for biomolecule absorption with different biomolecule layer thicknesses at the hotspot of a nanoantenna. We can see that with increasing biomolecule thickness, the peak wavelength red-shifts gradually. From the simulation, a biomolecular layer with a thickness of 4 nm causes a red shift of 7 nm in the peak wavelength. With a 30 min incubation in 500 nM streptavidin solution, it is expected that the streptavidin is saturated on the surface and that the biomolecule thickness is about 4 nm.[46] Our experimental result is in good agreement with the simulation.

The sensitivity of the hybrid nanoantennas depends strongly on the electric field confinement at the hotspots. Stronger field confinement will give rise to a higher sensitivity. In order to prove this, we tested the optical scattering spectra of the hybrid nanoantennas with a gap size of 45 nm in response to streptavidin exposure, as shown in Fig. 4. A much smaller peak shift of ~3 nm is observed compared to the case with a gap size of 20 nm, since the field intensity decreases dramatically with increasing gap size.

As a comparison, the optical scattering response for the gold nanorod array on streptavidin binding was also measured. In this case, the biotin functional group was introduced onto the gold surface by SH-PEG–biotin. After incubation in 500 nM streptavidin for 30 min, the whole Au nanorod surface was saturated with streptavidin molecules. A clear resonance red shift of 12 nm is observed as shown in Fig. 5.

In terms of the peak shift in the scattering spectra, the nanorods show a larger red shift than that of 20 nm hybrid nanoantennas in streptavidin detection, as shown in Fig. 6(a). However, considering the bioactive area is proportional to the number of bound molecules and the different bioactive surface area of the nanoantennas and nanorods, the optical response

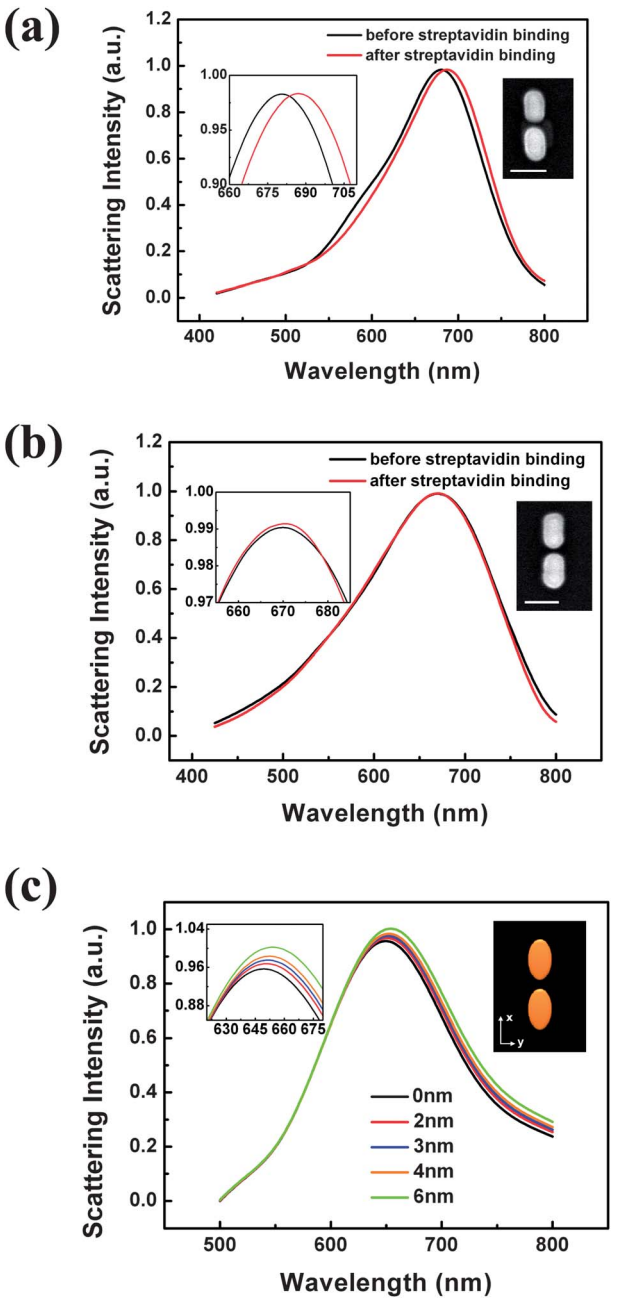

Fig. 3 Scattering spectra of nanoantenna arrays (a) with and (b) without Ti disks with a gap size of 20 nm before and after streptavidin binding, and (c) simulated scattering spectra of the hybrid nanoantenna array with different biomolecule layer thicknesses. Insets in (a) and (b) are the enlarged peaks and the SEM images of the nanoantenna used in the measurements. Insets in (c) are the enlarged peaks and the schematic of the simulation model. The scale bars in SEM images are 100 nm.

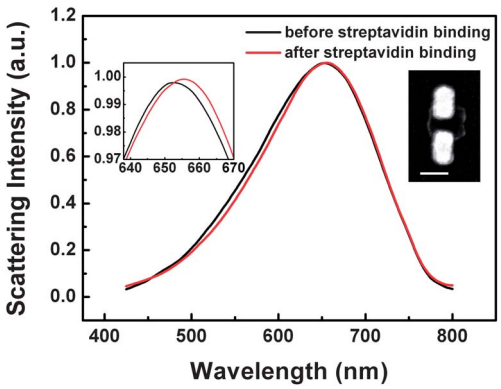

Fig. 4 Scattering spectra of the nanoantenna array with a gap size of 45 nm before and after streptavidin binding. Insets are the enlarged peaks and the SEM image. The scale bar in SEM image is 100 nm.

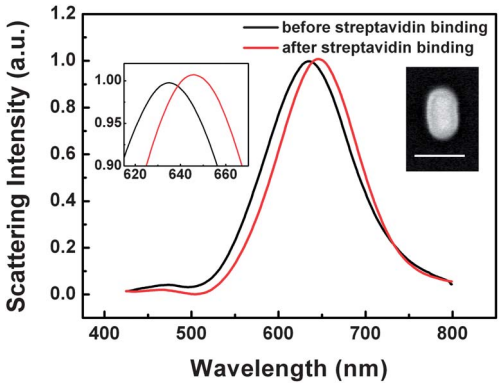

Fig. 5 Scattering spectra of the single nanorod array before and after streptavidin binding. Insets are the enlarged peaks and the SEM image. The scale bar in SEM image is 100 nm.

triggered per single molecule in the hybrid nanoantennas is actually much higher than that of the nanorod. In our experiments, the individual nanorod has a bioactive area about 10 times larger than the individual nanoantenna. The triggered signal per molecule for the 20 nm gap nanoantennas is actually 6 times higher than nanorods, as shown in Fig. 6(b). Even the 45 nm gap nanoantennas have a higher sensitivity per molecule than the nanorods, but the enhancement factor decreases as the gap size increases. At saturation response, the surface coverage by the streptavidin is 53%.[46] If approximating the streptavidin molecules as hard spheres with a diameter of 4 nm,[46] it is estimated that 350 streptavidin molecules were bound on each Ti disk in the case of the nanoantenna with a 20 nm gap. This is equivalent to a sensitivity of 0.023 nm peak wavelength shift per streptavidin molecule, which could be resolvable for a state-of-the-art spectrometer. In comparison to streptavidin selectively binding to a nanohole where molecular sensitivity is about 0.005 nm peak wavelength shift per streptavidin molecule,[35] our result is 4 times higher. Our molecular sensitivity is even higher than that of the silver sphere, which is 0.018 nm peak wavelength shift per streptavidin molecule.[47]

4. Conclusions

In summary, we have demonstrated an extremely high sensitivity in biosensing using hybrid plasmonic nanoantennas with selective biomolecule binding at the hotspots. With a materials-selective surface modification strategy and a proper selection of the hybrid nanoantenna composition materials of Au and Ti, streptavidin binding can be directed exclusively to the hotspots

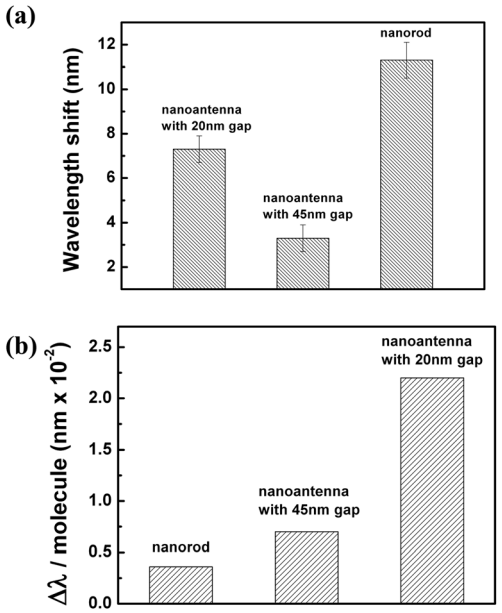

Fig. 6 (a) Comparison of wavelength shift introduced by streptavidin binding to different arrays and (b) corresponding sensitivity in wavelength shift per molecule.

of the nanoantenna. Both experimental and simulation results have confirmed that the localized electric field at the hotspots of the nanoantennas and the selective molecule binding are the key factors contributing to the enhanced sensitivity. The optical response of the nanoantennas in terms of peak wavelength red shift in the scattering spectra increases as the gap size decreases. The wavelength shift per molecule in 20 nm gap hybrid nanoantennas is enhanced by 6 times compared to that of nanorods. Our hybrid nanoantennas provide a very promising route towards future single-molecule detection.

Acknowledgements

This work was financially supported by Agency for Science, Technology and Research (A*STAR) under Grant nos 0921540099, 0921540098 and 12302FG012.

References

1 Y. Chen, K. Munechika and D. S. Ginger, *Nano Lett.*, 2007, **7**, 690.
2 J. R. Lakowicz, K. Ray, M. Chowdhury, H. Szmacinski, Y. Fu, J. Zhang and K. Nowaczyk, *Analyst*, 2008, **133**, 1308.
3 M. B. Reuben, P. D. Vladimir, L. Zhengtong, Y. Hsiao-Kuan, H. P. Rasmus, B. Alexandra, C. Jiji, I. Joseph, V. K. Alexander and M. S. Vladimir, *New J. Phys.*, 2008, **10**, 125022.
4 H. Szmacinski, R. Badugu and J. R. Lakowicz, *J. Phys. Chem. C*, 2010, **114**, 21142.
5 Z. Yi, X. Y. Li, F. J. Liu, P. Y. Jin, X. Chu and R. Q. Yu, *Biosens. Bioelectron.*, 2013, **43**, 308.
6 N. G. Greeneltch, M. G. Blaber, A. I. Henry, G. C. Schatz and R. P. Van Duyne, *Anal. Chem.*, 2013, **85**, 2297.
7 H. Ko, S. Singamaneni and V. V. Tsukruk, *Small*, 2008, **4**, 1576.
8 W. Yue, Y. Yang, Z. Wang, L. Chen and X. Wang, *Sens. Actuators, B*, 2012, **171–172**, 734.
9 E. Laux, C. Genet, T. Skauli and T. W. Ebbesen, *Nat. Photonics*, 2008, **2**, 161.
10 G. Si, Y. Zhao, H. Liu, S. Teo, M. Zhang, T. J. Huang, A. J. Danner and J. Teng, *Appl. Phys. Lett.*, 2011, **99**, 033105.
11 Y. J. Liu, G. Y. Si, E. S. P. Leong, N. Xiang, A. J. Danner and J. H. Teng, *Adv. Mater.*, 2012, **24**, OP131.
12 G. Si, Y. Zhao, J. Lv, M. Lu, F. Wang, H. Liu, N. Xiang, T. J. Huang, A. J. Danner, J. Teng and Y. J. Liu, *Nanoscale*, 2013, **5**, 6243.
13 W. Srituravanich, L. Pan, Y. Wang, C. Sun, D. B. Bogy and X. Zhang, *Nat. Nanotechnol.*, 2008, **3**, 733.
14 H. Liu, B. Wang, L. Ke, J. Deng, C. C. Chum, S. L. Teo, L. Shen, S. A. Maier and J. Teng, *Nano Lett.*, 2012, **12**, 1549.
15 W. Srituravanich, N. Fang, C. Sun, Q. Luo and X. Zhang, *Nano Lett.*, 2004, **4**, 1085.
16 S. Mubeen, G. Hernandez-Sosa, D. Moses, J. Lee and M. Moskovits, *Nano Lett.*, 2011, **11**, 5548.
17 N. Zhang, X. Su, P. Free, X. Zhou, K. G. Neoh, J. Teng and W. Knoll, *Sens. Actuators, B*, 2013, **183**, 310.
18 Y. N. Tan, X. Su, Y. Zhu and J. Y. Lee, *ACS Nano*, 2010, **4**, 5101.
19 T. Shegai and C. Langhammer, *Adv. Mater.*, 2011, **23**, 4409.
20 T. Klar, M. Perner, S. Grosse, G. von Plessen, W. Spirkl and J. Feldmann, *Phys. Rev. Lett.*, 1998, **80**, 4249.
21 M. Hu, A. Ghoshal, M. Marquez and P. G. Kik, *J. Phys. Chem. C*, 2010, **114**, 7509.
22 H. Xu, J. Aizpurua, M. Käll and P. Apell, *Phys. Rev. E: Stat. Phys., Plasmas, Fluids, Relat. Interdiscip. Top.*, 2000, **62**, 4318.
23 H. Fischer and O. J. F. Martin, *Opt. Express*, 2008, **16**, 9144.
24 E. Cubukcu, E. A. Kort, K. B. Crozier and F. Capasso, *Appl. Phys. Lett.*, 2006, **89**, 093120.
25 L. Cao, J. S. Park, P. Fan, B. Clemens and M. L. Brongersma, *Nano Lett.*, 2010, **10**, 1229.
26 J. Homola, *Chem. Rev.*, 2008, **108**, 462.
27 A. B. Dahlin, S. Chen, M. P. Jonsson, L. Gunnarsson, M. Käll and F. Höök, *Anal. Chem.*, 2009, **81**, 6572.
28 P. Kvasnička and J. Homola, *Biointerphases*, 2008, **3**, FD4.
29 K. H. Chen, J. Hobley, Y. L. Foo and X. Su, *Lab Chip*, 2011, **11**, 1895.
30 T. Rindzevicius, Y. Alaverdyan, A. Dahlin, F. Höök, D. S. Sutherland and M. Käll, *Nano Lett.*, 2005, **5**, 2335.
31 G. J. Nusz, S. M. Marinakos, A. C. Curry, A. Dahlin, F. Hook, A. Wax and A. Chilkoti, *Anal. Chem.*, 2008, **80**, 984.
32 S. K. Dondapati, T. K. Sau, C. Hrelescu, T. A. Klar, F. D. Stefani and J. Feldmann, *ACS Nano*, 2010, **4**, 6318.
33 L. Guo and D. H. Kim, *Biosens. Bioelectron.*, 2012, **31**, 567.
34 A. I. Henry, J. M. Bingham, E. Ringe, L. D. Marks, G. C. Schatz and R. P. Van Duyne, *J. Phys. Chem. C*, 2011, **115**, 9291.
35 J. Ferreira, M. J. L. Santos, M. M. Rahman, A. G. Brolo, R. Gordon, D. Sinton and E. M. Girotto, *J. Am. Chem. Soc.*, 2008, **131**, 436.

36 L. Feuz, P. Jönsson, M. P. Jonsson and F. Höök, *ACS Nano*, 2010, **4**, 2167.
37 A. Nanci, J. D. Wuest, L. Peru, P. Brunet, V. Sharma, S. Zalzal and M. D. McKee, *J. Biomed. Mater. Res.*, 1998, **40**, 324.
38 E. D. Palik, *Handbook of Optical Constants of Solids*, Elsevier Science, 1997.
39 P. B. Johnson and R. W. Christy, *Phys. Rev. B: Solid State*, 1972, **6**, 4370.
40 L. Niu and W. Knoll, *Anal. Chem.*, 2007, **79**, 2695.
41 J. Spinke, M. Liley, F. J. Schmitt, H. J. Guder, L. Angermaier and W. Knoll, *J. Chem. Phys. C*, 1993, **99**, 7012.
42 G. L. Kenausis, J. Vörös, D. L. Elbert, N. Huang, R. Hofer, L. Ruiz-Taylor, M. Textor, J. A. Hubbell and N. D. Spencer, *J. Phys. Chem. B*, 2000, **104**, 3298.
43 M. Rodenstein, S. Zurcher, S. G. Tosatti and N. D. Spencer, *Langmuir*, 2010, **26**, 16211.
44 B. Malisova, S. Tosatti, M. Textor, K. Gademann and S. Zurcher, *Langmuir*, 2010, **26**, 4018.
45 L. Feuz, M. P. Jonsson and F. Höök, *Nano Lett.*, 2012, **12**, 873.
46 W. Knoll, M. Zizlsperger, T. Liebermann, S. Arnold, A. Badia, M. Liley, D. Piscevic, F. J. Schmitt and J. Spinke, *Colloids Surf., A*, 2000, **161**, 115.
47 A. J. Haes, D. A. Stuart, S. Nie and R. P. Van Duyne, *J. Fluoresc.*, 2004, **14**, 355.